Electronic Supplementary Information for

Convenient Synthesis of Copper(I) Halide Quasi-One-Dimensional Coordination Polymers: Their Structures and Solid-State Luminescent Properties

Shingo Masahara,[†a] Hiromichi Yokoyama,[†a] Yuji Suzaki,[b] Tomohito Ide*[a]

[a.] *Department of Chemical Science and Technology, National Institute of Technology, Tokyo College, 1220-2 Kunugida-machi, Hachioji-shi, Tokyo, 193-0997, Japan*

[b.] *Laboratory for Chemistry and Life Science, Institute of Innovative Research, Tokyo Institute of Technology, 4259-R1-3 Nagatsuta, Midori-ku, Yokohama 226-8503, Japan.*

[†] These authors contributed equally to this work.

Email: ide@tokyo-ct.ac.jp

Table of Contents

1. Examined Pyridines

Table S1 Examined pyridine ligands for the reaction in suspension.

CuX	Ligand	Luminescence color	Yield[a] (%)	Reference
CuCl	2-bromopyridine	No luminescence	86	This work
	2-vinylpiridine	Yellow	70	S1 [b,i]
	3,5-dimethylpyridine	Green	108	S2 [g]
	3-aminopyridine	Yellow	82	S3 [h]
	3-bromopyridine	Green	97	This work
	3-methoxypyridine	Green	88	This work
	3-vinylpiridine	No luminescence	86	This work
	4-cyanopyridine	Yellow	102	S4,[d,i] S5,[h] S6 [h]
	isoquinoline	No luminescence	57	S7 [h]
	nicotinamide	Blue	117	This work
	pyridine	No luminescence	78	S7,[h] S8 [c]
CuBr	3-bromopyridine	Blue-green	82	S9,[c] S10 [c,j]
	3-methoxypyridine	No luminescence	87	This work
	3,5-dimethylpyridine	Green	77	S2,[g,i] S9,[e] S10 [f,j]
CuI	3-bromopyridine	Blue	90	S9,[c] S11 [c,i]
	3-methoxypyridine	No luminescence	96	This work
	3,5-dimethylpyridine	Blue	89	S2,[g,i] S9,[e] S11,[f,j] S12 [f,j]

[a] Assuming the molar ratio of CuX and ligand to be 1:1. The yields over 100% indicate CuX reacted with ligands more than one equivalent.

[b] 1D CP with rhomboidal Cu_2X_2 and ligand unit.

[c] 1D stair-shaped CP (ligands are in a parallel position).

[d] 3D CP with Cu(I) ion linked with 4-cyanopyridine and chloride ligand.

[e] Rhomboidal dinuclear complex.

[f] 1D ladder-like CP.

[g] Tetrahedral mononuclear complex.

[h] X-ray structure was not reported.

[i] Calculated PXRD pattern from the X-ray structure reported in the literature is not matched to the measured pattern of obtained powder in this work.

[j] Calculated PXRD pattern from the X-ray structure reported in the literature is identical to the measured pattern of obtained powder in this work.

1.1. Synthetic Procedures

CuCl(2-BrPy) powder. CuCl (0.106 g, 1.1 mmol), ethyl acetate (3 mL), and 2-bromopyridine (0.326 g, 2.1 mmol) were used. A white powder (0.236 g), which not showed an emission under UV light was obtained.

CuCl(3-H_2CCHPy) powder. CuCl (0.103 g, 1.0 mmol), ethyl acetate (3 mL), and 3-vinylpyridine (0.196 g, 1.9 mmol) were used. A white powder (0.182 g), which not showed an emission under UV light was obtained.

CuCl(Py) powder. CuCl (0.104 g, 1.1 mmol), ethyl acetate (3 mL), and pyridine (0.147 g, 1.9 mmol) were used. A green powder (0.146 g), which not showed an emission under UV light was obtained.

CuCl(isoquinoline) powder. CuCl (0.104 g, 1.1 mmol), ethyl acetate (3 mL), and isoquinoline (0.219 g, 1.7 mmol) were used. A grey powder (0.137 g), which not showed an emission under UV light was obtained.

CuBr(3-MeOPy) powder. CuBr (0.146 g, 1.0 mmol), ethyl acetate (3 mL), and 3-methoxypyridine (0.216 g, 2.0 mmol) were used. A green powder (0.221 g), which not showed an emission under UV light was obtained.

CuI(3-MeOPy) powder. CuI (0.195 g, 1.0 mmol), ethyl acetate (3 mL), and 3-methoxypyridine (0.216 g, 2.0 mmol) were used. A white powder (0.288 g), which not showed an emission under UV light was obtained.

Those compound that does not exhibit luminescence was not considered in detail.

2. Effect of equivalents of pyridine ligand

In the case of synthesis using 3-methoxypyridine and 3,5-dimethylpyridine, no CuCl peaks were observed in PXRD measurements. However, TG measurements showed multistep decomposition, indicating the formation of multiple compounds. The synthesis was carried out by changing the equivalent of the pyridine ligand.

Table S2 Effect of equivalents of pyridine ligand

Ligand	Equivalents of pyridine ligand	Estimated structure $CuCl(L)_n$[b]	Luminescence color	Yield[c] (%)	CuX:ligand ratio[b]
3-methoxypyridine	1.9[a]	CuCl(3,5-MeOPy)	Green	88	1.0:0.66
	2.7	CuCl(3,5-MeOPy)	Green	67	1.0:0.80
	3.9	CuCl(3,5-MeOPy)	Green	55	1.0:0.56
3,5-dimethylpyridine	1.6[a]	$CuCl(3,5\text{-}Me_2Py)$	Green	108	1.0:2.5
	1.0	$CuCl(3,5\text{-}Me_2Py)$	Green	64	1.0:0.75
	3.6	$CuCl(3,5\text{-}Me_2Py)_3$	Yellow-green	80	1.0:2.7

[a] Described in the main text.

[b] Determined from TG measurement.

[c] Assuming the molar ratio of CuX and ligand to be 1:*n*. The value of *n* is taken from the estimated structure. The yields over 100% indicate CuX reacted with ligands more than *n* equivalent.

In the case of CuCl(3-MeOPy), 2.7 equivalents of 3-methoxypyridine were used. Increasing equivalents of the ligand did not affect TG curve shape. However, the molar ratio between CuX and ligand increased to 1:0.80. (see Figure S31). The PXRD pattern of the products matched with the simulated pattern of CuCl(3-MeOPy) CP (see Figure S1), which indicates mainly gave stair-shaped CP. Further investigation for the reaction with 3.9-equivalent of the 3-methoxypyrdine presented lower yields (55%) and molar ratio CuX:ligand = 1:0.56 (see Figure S31). PXRD analysis revealed remaining CuCl in a product (Figure S1). These results suggested the formation of mononuclear complex (or oligonuclear complex) with a higher ligand ratio compared with quasi-1D CP, which is able to dissolve in ethyl acetate.

In the case of $CuCl(3,5\text{-}Me_2Py)$, the equivalents of the ligand were modified to 1.0 or 3.6. When 1.0 equivalents of 3,5-dimethylpyridine was used, the reaction mainly gave a ladder-like complex based on the X-ray analyses. However, remained CuCl was also observed. The TG curve suggested multistep decompositions, and the calculated molar ratio of CuX:ligand was 1:0.75 (see Figure S32). When 3.6 equivalents of 3,5-dimethylpyridine were used, a mononuclear complex was mainly obtained. The TG analysis revealed that the CuX:ligand ratio was 1:2.7 and suggested multistep decomposition. The shape of the TG curve is almost the same as the powder obtained by reaction with 1.6 equivalents of 3,5-dimethylpyridine except for total weight loss (See Figure S32). The mononuclear complex with 3,5-dimethylpyridine was slightly dissolved in ethyl acetate. The dissolved complex was easily oxidised and discoloured. Since the complex is not dissolved in hexane, the obtained powder was washed with hexane instead of ethyl acetate.

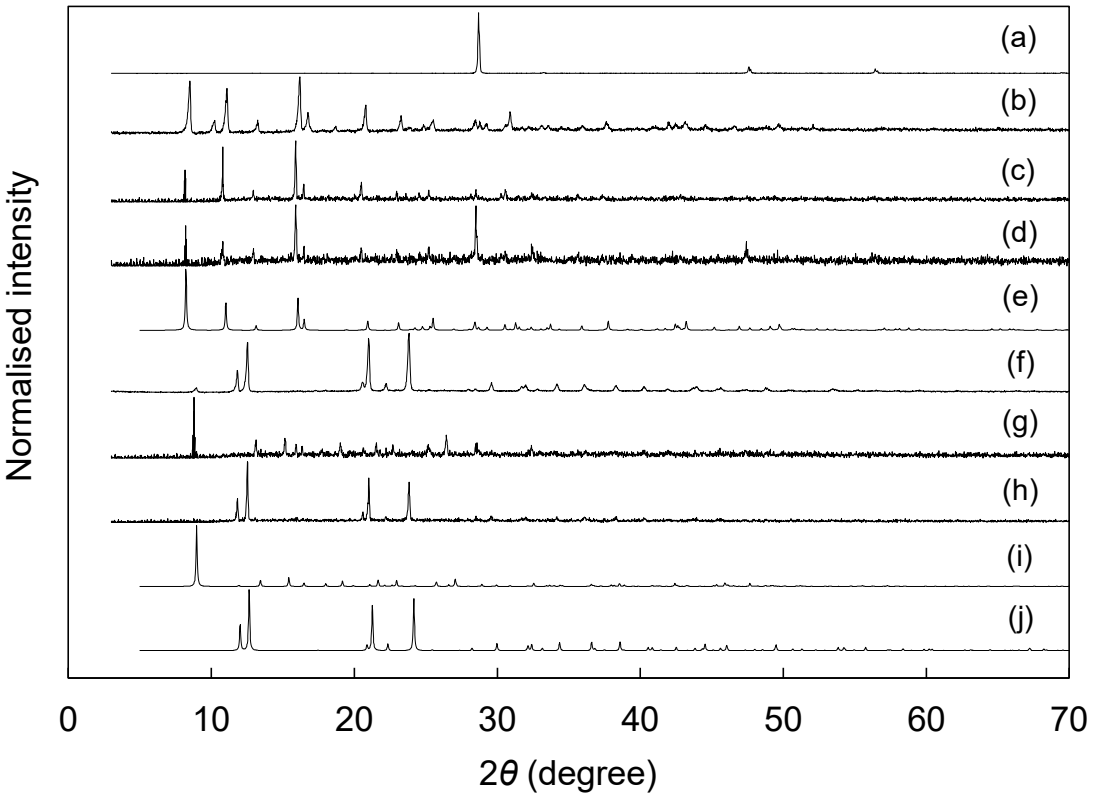

Figure S1 PXRD patterns of (a) CuCl, (b) CuCl(3-MeOPy) powder obtained with 1.9 eq. of 3-methoxypyridine in suspension, (c) with 2.7 eq. in suspension, (d) with 3.9 eq. in suspension, (e) simulated pattern of CuCl(3-MeOPy) CP, (f) CuCl(3,5-Me_2Py) powder obtained with 1.6 eq. of 3,5-dimethylpyridine in suspension, (g) with 1.0 eq. in suspension, (h) with 3.6 eq. in suspension, (i) simulated pattern of CuCl(3,5-Me_2Py) CP, (j) simulated pattern of CuCl(3,5-Me_2Py) mononuclear complex.

2.1. Synthetic procedures

CuCl(3-MeOPy) powder (2.7 eq. of the ligand). CuCl (0.107 g, 1.1 mmol), ethyl acetate (3 mL), and 3-methoxypyridine (0.324 g, 3.0 mmol) were used. A green powder (0.153 g), which showed a green emission under UV light was obtained. FT-IR (KBr): 3097.1, 3070.4, 3057.6, 2976.4, 2945.7, 2838.2, 2514.0, 2090.7, 2044.2, 2016.9, 1938.6, 1888.9, 1885.6, 1868.9, 1601.6, 1577.7, 1559.9, 1480.3, 1456.5, 1431.7, 1290.6, 1236.9, 1198.3, 1176.6, 1151.5, 1136.6, 1114.9, 1060.2, 1031.3, 1012.9, 913.1, 900.4, 854.1, 812.1, 799.1, 792.4, 697.4, 460.7 cm^{-1}.

CuCl(3-MeOPy) powder (3.9 eq. of the ligand). CuCl (0.0995 g, 1.0 mmol), ethyl acetate (3 mL), and 3-methoxypyridine (0.432 g, 4.0 mmol) were used. A green powder (0.116 g), which showed a green emission under UV light was obtained. FT-IR (KBr): 3852.1, 3397.0, 3058.6, 2975.6, 2943.8, 2837.7, 1601.6, 1577.5, 1480.6, 1431.4, 1290.1, 1237.1, 1203.4, 1177.8, 1136.8, 1114.7, 1060.2, 1031.3, 1012.5, 900.6, 852.4, 807.1, 798.9, 792.6, 697.1, 650.4, 640.7, 571.8 cm^{-1}.

CuCl(3,5-Me$_2$Py) powder (1.0 eq. of the ligand). CuCl (0.108 g, 1.1 mmol), ethyl acetate (3 mL), and 3,5-dimethylpyridine (0.113 g, 1.1 mmol) were used. A white powder (0.145 g), which showed a green emission under UV light was obtained. FT-IR (KBr): 3010.1, 2950.7, 2914.9, 2863.3, 2746.4, 2490.9, 1598.9, 1576.0, 1559.9, 1538.9, 1521.1, 1506.9, 1496.0, 1464.9, 1436.7, 1378.3, 1322.2, 1283.6, 1243.4, 1173.5, 1148.2, 1048.4, 1037.0, 1023.8, 924.9, 904.7, 865.4, 808.3, 776.0, 758.1, 702.0 cm^{-1}.

CuCl(3,5-Me$_2$Py) powder (3.6 eq. of the ligand). CuCl (0.103 g, 1.1 mmol), ethyl acetate (3 mL), and 3,5-dimethylpyridine (0.418 g, 3.9 mmol) were used. This powder washed with hexane instead of ethyl acetate. A green powder (0.350 g), which showed a yellow-green emission under UV light was obtained. FT-IR (KBr): 3032.5, 3020.9, 2953.0, 2917.3, 2686.8, 2743.7, 2489.2, 1595.3, 1463.2, 1422.7, 1387.5, 1379.3, 1325.3, 1243.4, 1177.8, 1171.5, 1147.9, 1048.1, 1033.7, 870.7, 775.2, 747.3, 708.2 cm^{-1}.

3. Crystallographic Parameters

Table S3 Crystallographic parameters of CuI(3-BrPy) CP.

	CuI(3-BrPy) CP
CCDC number	2053630
Formula	$C_5H_4BrCuIN$
Fw	348.44
Size of crystal/mm	0.518 × 0.101 × 0.06
Crystal System	orthorhombic
Space Group	$P2_12_12_1$ (no. 19)
a/Å	4.0975(2)
b/Å	11.5751(6)
c/Å	16.3426(8)
α/°	90
β/°	90
γ/°	90
V/Å^3	775.11(7)
Z	4
D_{calc}/g cm^{-3}	2.986
F(000)	632.0
No. of reflections measured	2498
No. of unique reflections	1329
No. of observations	1308
R ($I > 2.0\sigma(I)$)	0.0315
R_w (all data)	0.0792
Goodness of fit	1.065

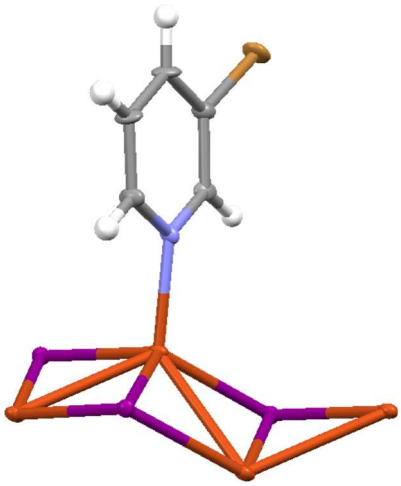

Figure S2 Thermal ellipsoid plot (50%) of CuI(3-BrPy) CP: (orange ball) Cu; (brown ball) Br; (purple ball) I; (blue ball) N; (grey ball) C; (white ball) H.

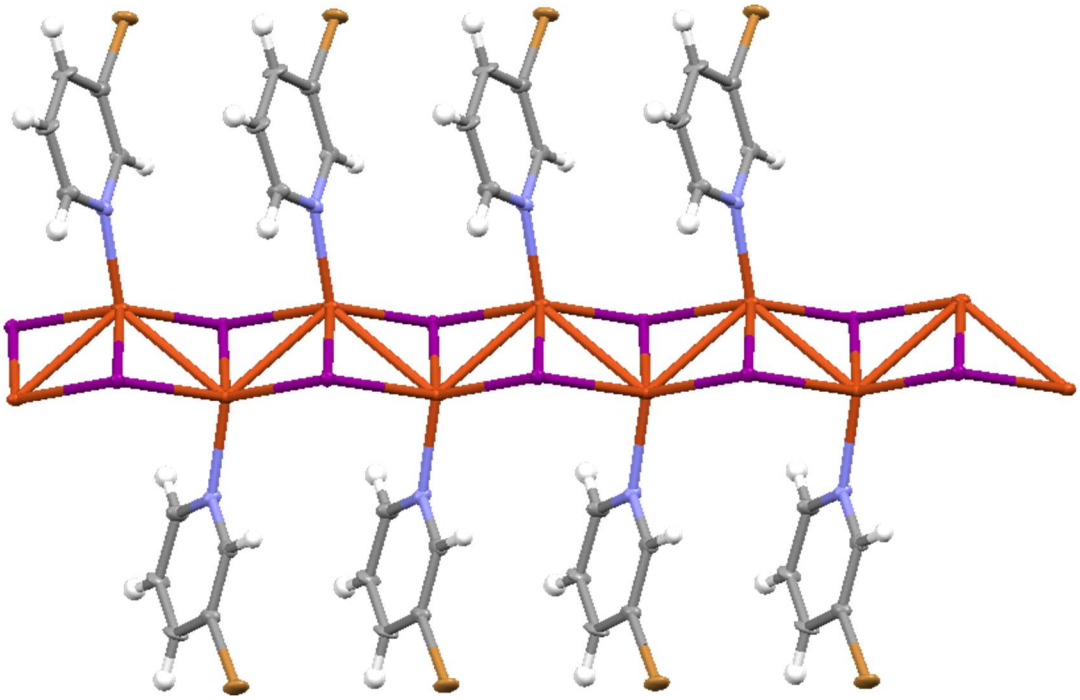

Figure S3 Thermal ellipsoid plot (50%) of expanded structure of CuI(3-BrPy) CP: (orange ball) Cu; (brown ball) Br; (purple ball) I; (blue ball) N; (grey ball) C; (white ball) H.

Table S4 Crystallographic parameters of CuBr(3-BrPy) CP.

	CuBr(3-BrPy) CP
CCDC number	2053631
Formula	$C_5H_4Br_2CuN$
Fw	301.45
Size of crystal/mm	0.616 × 0.081 × 0.041
Crystal System	monoclinic
Space Group	$P2_1/n$ (No. 14)
a/Å	8.7546(3)
b/Å	3.91060(10)
c/Å	21.0487(7)
α/°	90
β/°	100.957(4)
γ/°	90
V/Å^3	707.48(4)
Z	3
D_{calc}/g cm^{-3}	2.830
F(000)	560.0
No. of reflections measured	3394
No. of unique reflections	1406
No. of observations	1353
R ($I > 2.0\sigma(I)$)	0.0352
R_w (all data)	0.0941
Goodness of fit	1.152

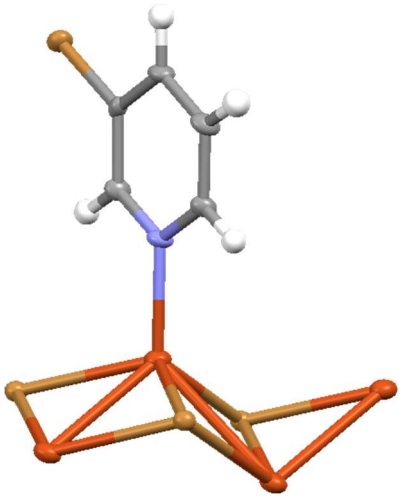

Figure S4 Thermal ellipsoid plot (50%) of CuBr(3-BrPy) CP: (orange ball) Cu; (brown ball) Br; (blue ball) N; (grey ball) C; (white ball) H.

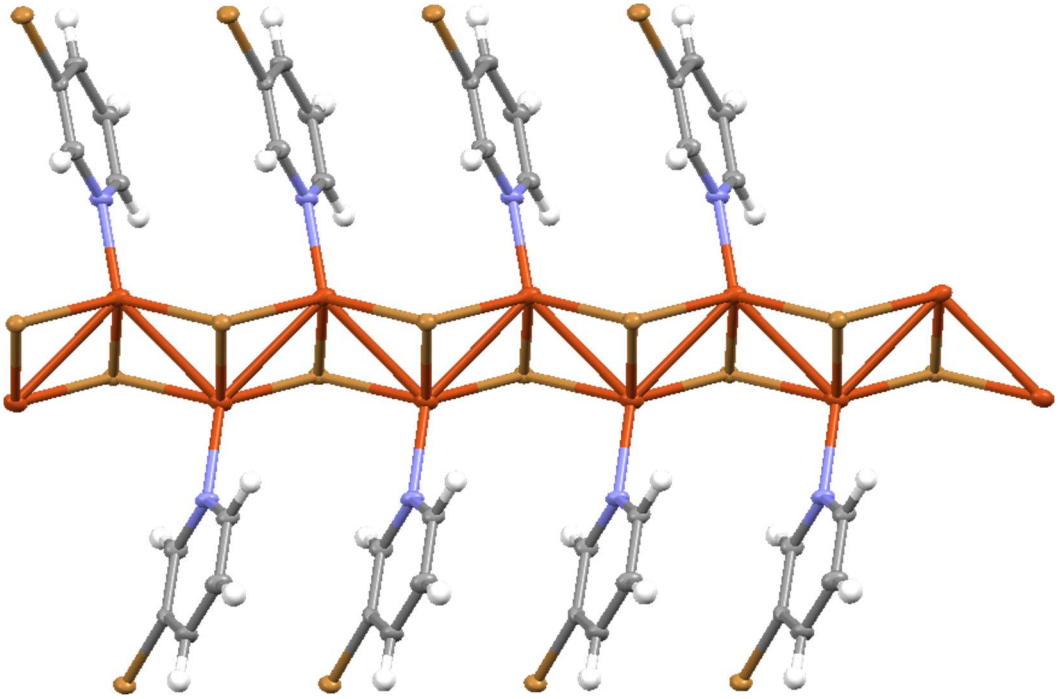

Figure S5 Thermal ellipsoid plot (50%) of expanded structure of CuBr(3-BrPy) CP: (orange ball) Cu; (brown ball) Br; (blue ball) N; (grey ball) C; (white ball) H.

Table S5 Crystallographic parameters of CuCl(3-MeOPy) CP.

	CuCl(3-MeOPy) CP
CCDC number	2053632
Formula	$C_{12}H_{14}Cl_2Cu_2N_2O_2$
Fw	416.23
Size of crystal/mm	0.333 × 0.082 × 0.055
Crystal System	orthorhombic
Space Group	$Pca2_1$ (no. 29)
a/Å	17.2967(9)
b/Å	3.8127(2)
c/Å	21.4776(11)
α/°	90
β/°	90
γ/°	90
V/Å^3	1416.39(13)
Z	4
D_{calc}/g cm^{-3}	1.952
F(000)	832.0
No. of reflections measured	4323
No. of unique reflections	2101
No. of observations	1946
R ($I > 2.0\sigma(I)$)	0.0331
R_w (all data)	0.0942
Goodness of fit	1.081

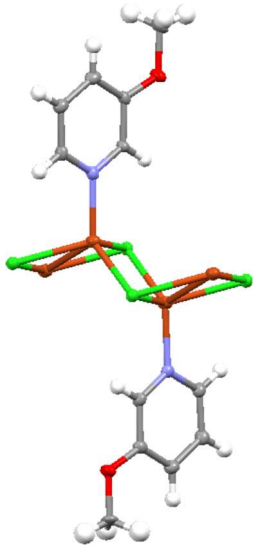

Figure S6 Thermal ellipsoid plot (50%) of CuCl(3-MeOPy) CP: (orange ball) Cu; (yellow-green ball) Cl; (red ball) O; (blue ball) N; (grey ball) C; (white ball) H.

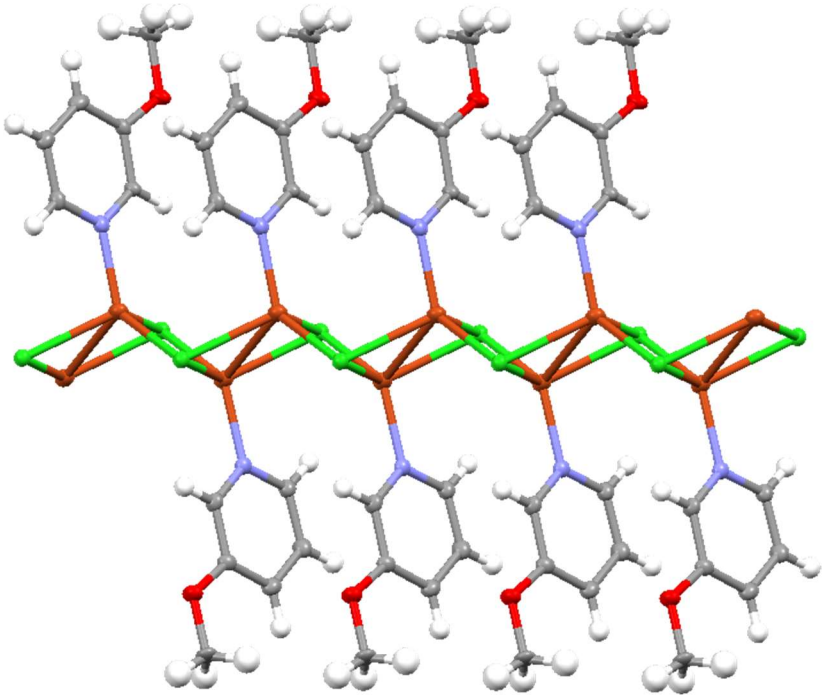

Figure S7 Thermal ellipsoid plot (50%) of expanded structure of CuCl(3-MeOPy) CP: (orange ball) Cu; (yellow-green ball) Cl; (red ball) O; (blue ball) N; (grey ball) C; (white ball) H.

Table S6 Crystallographic parameters of CuCl(3,5-Me_2Py) CP.

	CuCl(3,5-Me_2Py) CP
CCDC number	2053633
Formula	C_7H_9ClCuN
Fw	206.14
Size of crystal/mm	0.561 × 0.142 × 0.074
Crystal System	monoclinic
Space Group	*C*2/c (No. 15)
a/Å	13.4029(5)
b/Å	14.8238(6)
c/Å	7.9397(3)
α/°	90
β/°	100.657(4)
γ/°	90
V/Å^3	1550.27(11)
Z	8
D_{calc}/g cm^{-3}	1.766
F(000)	832.0
No. of reflections measured	4657
No. of unique reflections	1500
No. of observations	1549
R (*I* > 2.0*σ*(*I*))	0.0325
R_w (all data)	0.0893
Goodness of fit	1.118

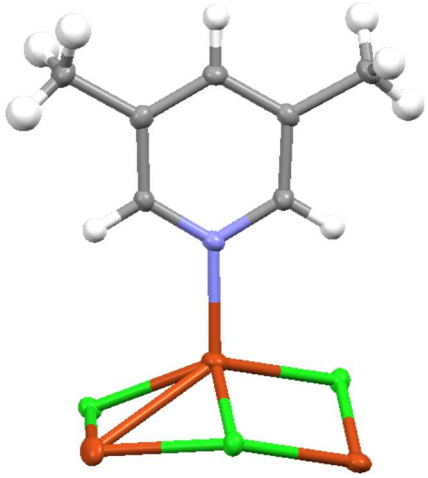

Figure S8 Thermal ellipsoid plot (50%) of CuCl(3,5-Me_2Py) CP: (orange ball) Cu; (yellow-green ball) Cl; (blue ball) N; (grey ball) C; (white ball) H.

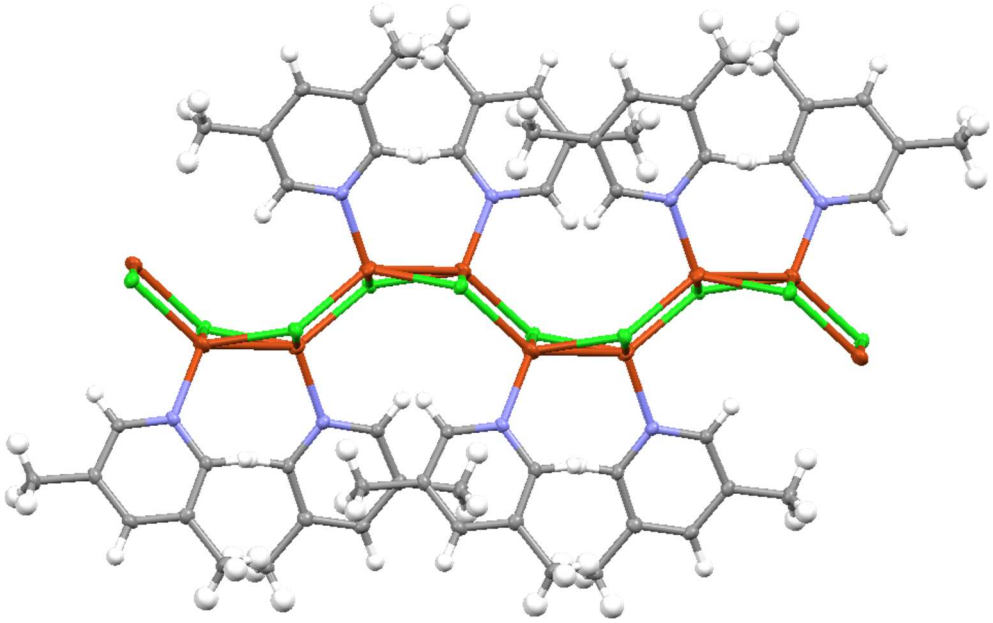

Figure S9 Thermal ellipsoid plot (50%) of expanded structure of CuCl(3,5-Me_2Py) CP: (orange ball) Cu; (yellow-green ball) Cl; (blue ball) N; (grey ball) C; (white ball) H.

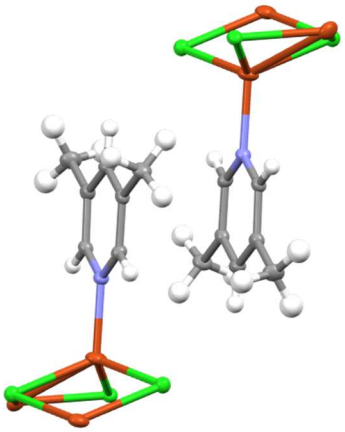

Figure S10 Thermal ellipsoid plot (50%) of stacking structure of CuCl(3,5-Me_2Py) CP: (orange ball) Cu; (yellow-green ball) Cl; (blue ball) N; (grey ball) C; (white ball) H.

Table S7 Crystallographic parameters of CuCl(3,5-Me_2Py).

	CuCl(3,5-Me_2Py)
CCDC number	2053634
Formula	$(C_{21}H_{27}ClCuN)_3$
Fw	1261.33
Size of crystal/mm	0.484 × 0.403 × 0.314
Crystal System	trigonal
Space Group	*R*3/*m* (No. 160)
a/Å	14.7196(5)
b/Å	14.7196(5)
c/Å	8.3670(4)
α/°	90
β/°	90
γ/°	120
V/Å^3	1569.97(13)
Z	1
D_{calc}/g cm^{-3}	1.334
F(000)	660.0
No. of reflections measured	1562
No. of unique reflections	679
No. of observations	679
R ($I > 2.0\sigma(I)$)	0.0170
R_w (all data)	0.0456
Goodness of fit	1.124

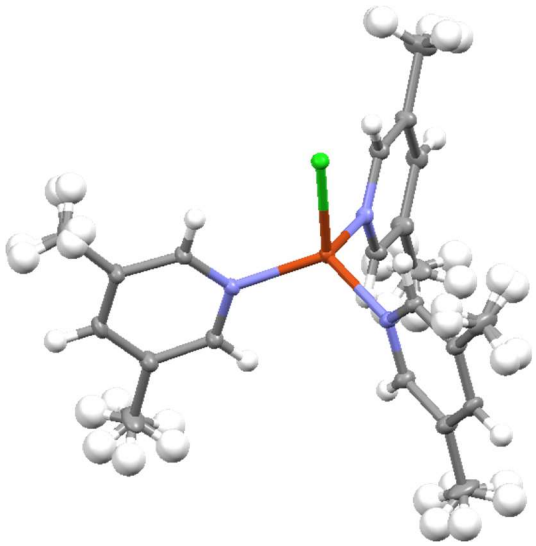

Figure S11 Thermal ellipsoid plot (50%) of CuCl(3,5-Me_2Py)$_3$: (orange ball) Cu; (yellow-green ball) Cl; (blue ball) N; (grey ball) C; (white ball) H.

Table S8 Crystallographic parameters of CuCl(3-BrPy) CP.

	CuCl(3-BrPy) CP
CCDC Number	2053635
Formula	$C_5H_4BrClCuN$
Fw	256.99
Size of crystal/mm	0.147 × 0.049 × 0.006
Crystal System	triclinic
Space Group	*P-1* (No. 2)
a/Å	3.836(3)
b/Å	8.624(7)
c/Å	10.449(9)
α/°	103.776(12)
β/°	93.709(14)
γ/°	90.104(12)
V/Å^3	335.0(5)
Z	2
D_{calc}/g cm^{-3}	2.548
F(000)	244.0
No. of reflections measured	2680
No. of unique reflections	1464
No. of observations	1156
R ($I > 2.0\sigma(I)$)	0.0329
R_w (all data)	0.0895
Goodness of fit	1.042

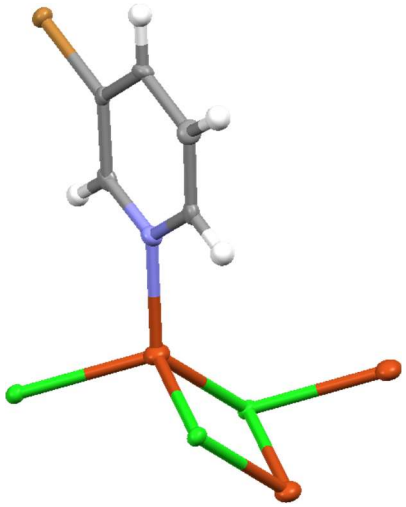

Figure S12 Thermal ellipsoid plot (50%) of CuCl(3-BrPy) CP: (orange ball) Cu; (yellow-green ball) Cl; (brown ball) Br; (blue ball) N; (grey ball) C; (white ball) H.

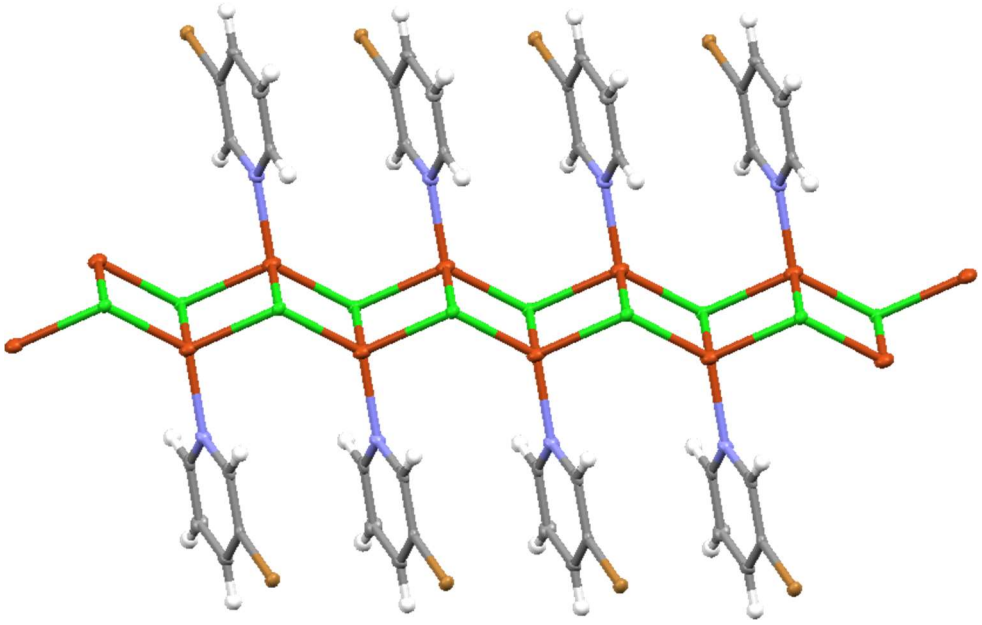

Figure S13 Thermal ellipsoid plot (50%) of expanded structure of CuCl(3-BrPy) CP: (orange ball) Cu; (yellow-green ball) Cl; (brown ball) Br; (blue ball) N; (grey ball) C; (white ball) H.

4. IR spectra

Table S9 IR absorption peaks attributed to aromatic bond stretch.

CuX	Ligand	Free ligand (cm^{-1})	Complex (cm^{-1})
CuCl	nicotinamide	1679, 1618	1697, 1620
	3-aminopyridine	1635, 1588	1629, 1583
	4-cyanopyridine	1589, 1564	1589, 1565
	2-vinylpyridine	1631, 1587	1635, 1570
	3-bromopyridine	1570, 1558	1583, 1556
	3-methoxypyridine	1600, 1580	1601, 1578
	3,5-dimethylpyridine	1600, 1580	1594, 1576
CuBr	3-bromopyridine	1570, 1558	1582, 1556
	3,5-dimethylpyridine	1580, 1557	1595, 1576
CuI	3-bromopyridine	1570, 1558	1583, 1555
	3,5-dimethylpyridine	1580, 1557	1595, 1577

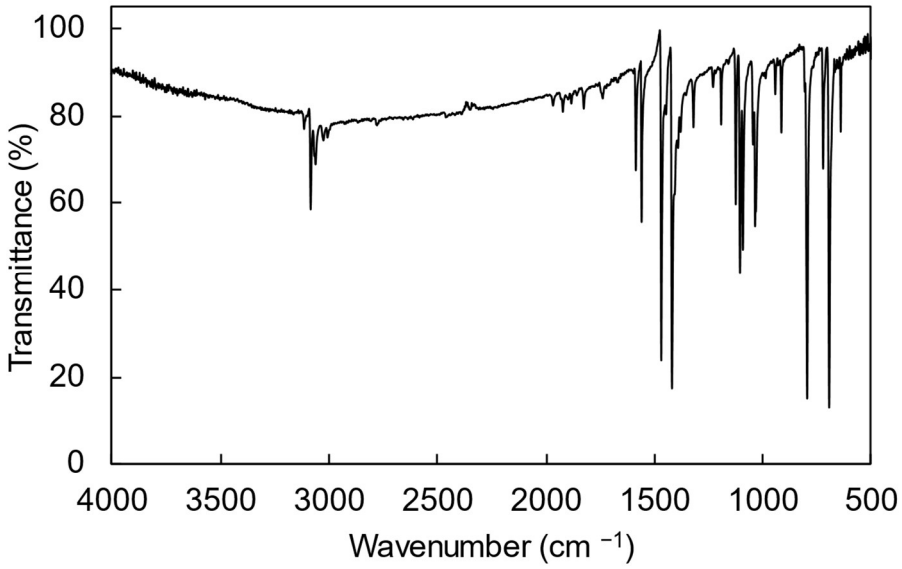

Figure S14 FT-IR spectra (KBr) of the CuCl(3-BrPy) powder prepared by the reaction in suspension.

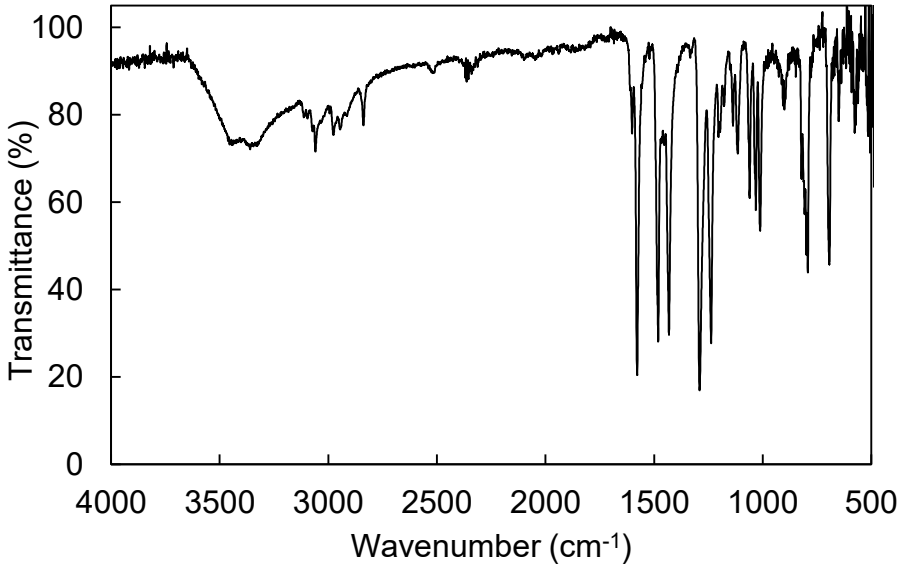

Figure S15 FT-IR spectra (KBr) of the CuCl(3-MeOPy) powder prepared by the reaction in suspension.

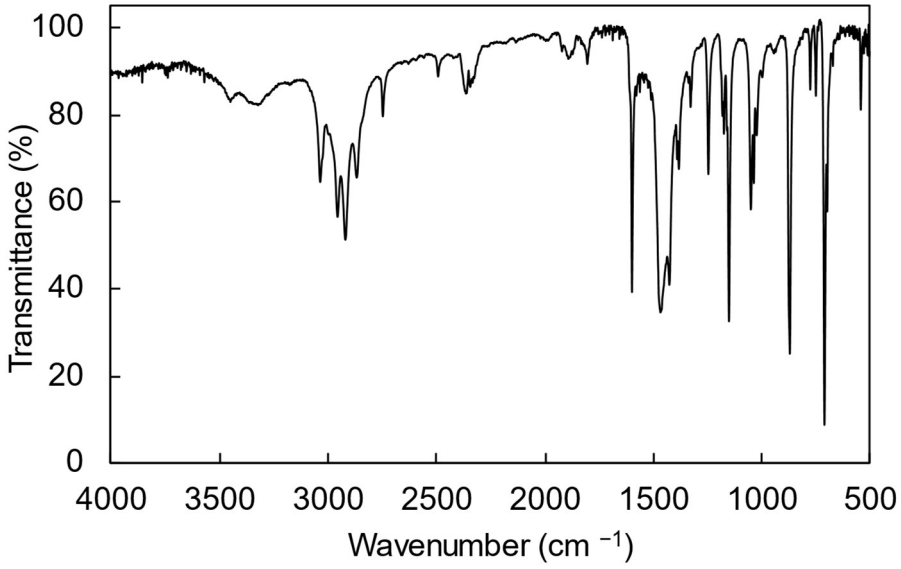

Figure S16 FT-IR spectra (KBr) of the CuCl(3,5-Me_2Py) powder prepared by the reaction in suspension.

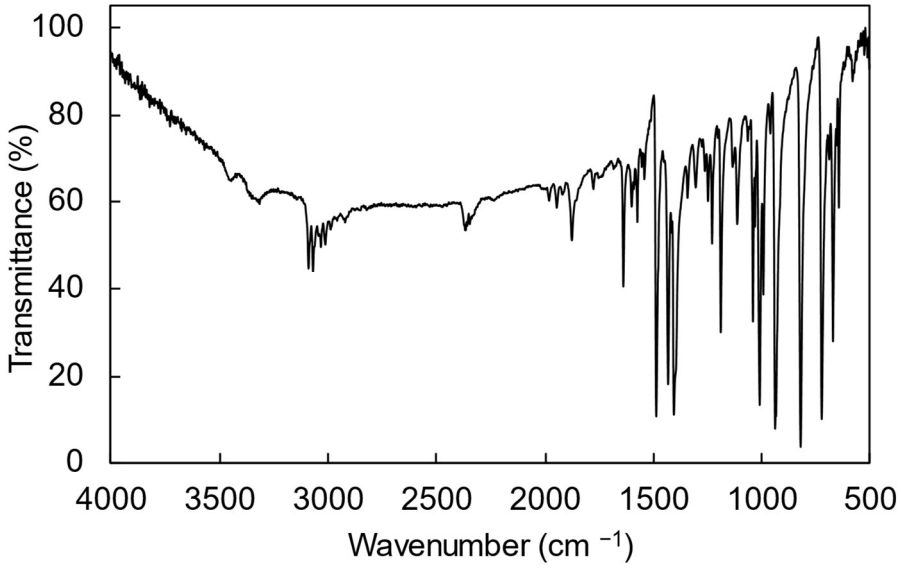

Figure S17 FT-IR spectra (KBr) of the CuCl(2-H_2CCHPy) powder prepared by the reaction in suspension.

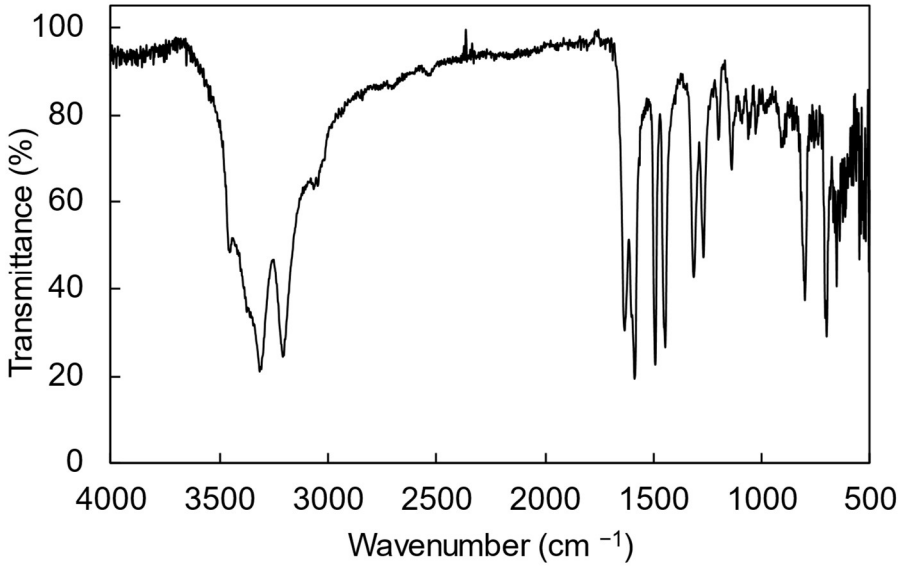

Figure S18 FT-IR spectra (KBr) of the CuCl(3-NH_2Py) powder prepared by the reaction in suspension.

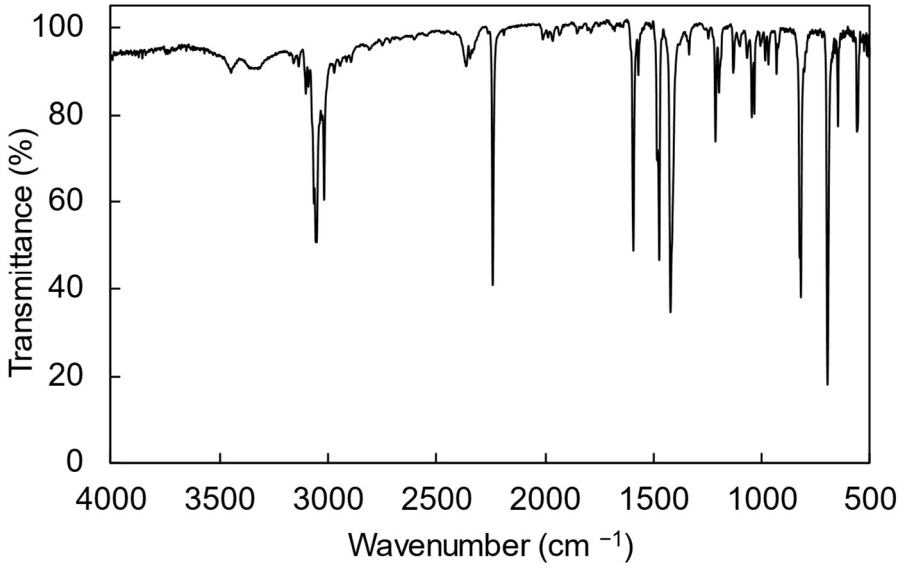

Figure S19 FT-IR spectra (KBr) of the CuCl(4-CNPy) powder prepared by the reaction in suspension.

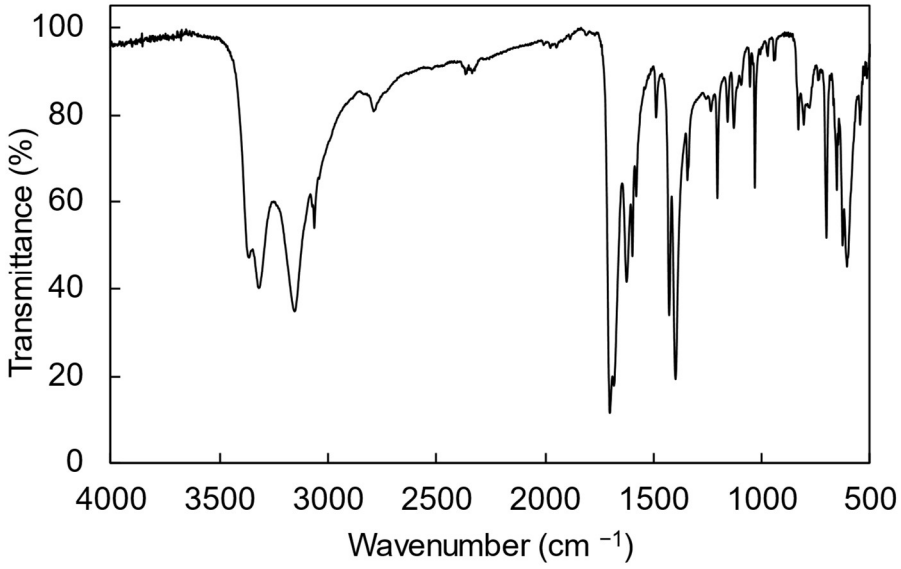

Figure S20 FT-IR spectra (KBr) of the CuCl(3-H_2NCOPy) powder prepared by the reaction in suspension.

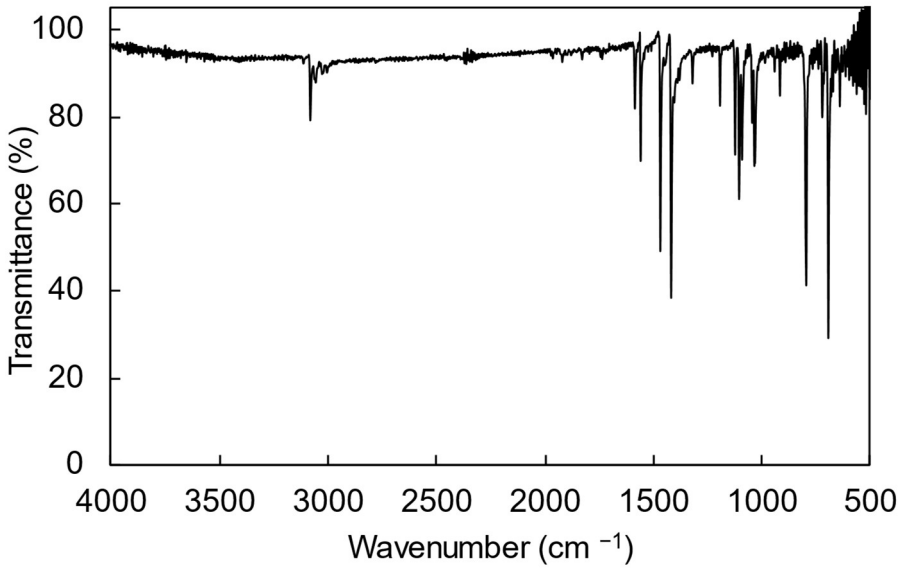

Figure S21 FT-IR spectra (KBr) of the CuBr(3-BrPy) powder prepared by the reaction in suspension.

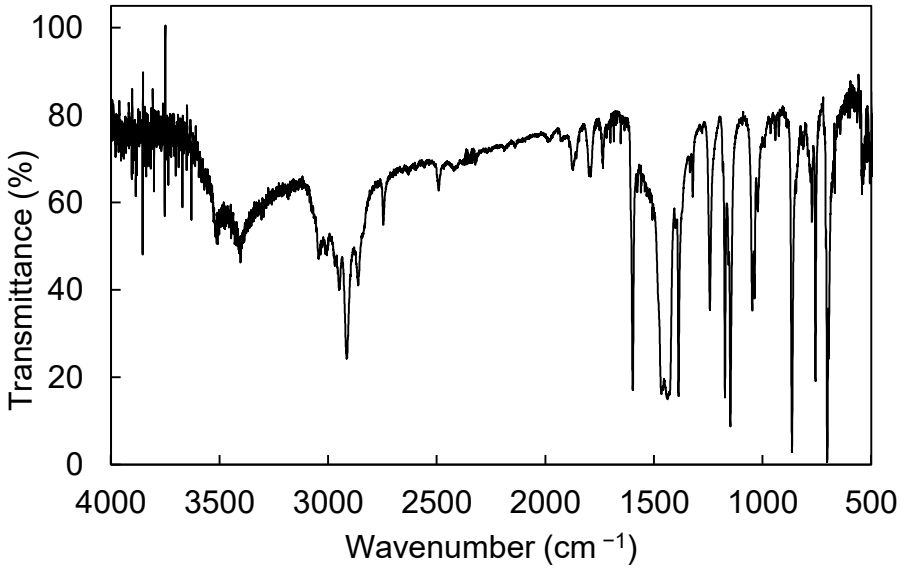

Figure S22 FT-IR spectra (KBr) of the CuBr(3,5-Me_2Py) powder prepared by the reaction in suspension.

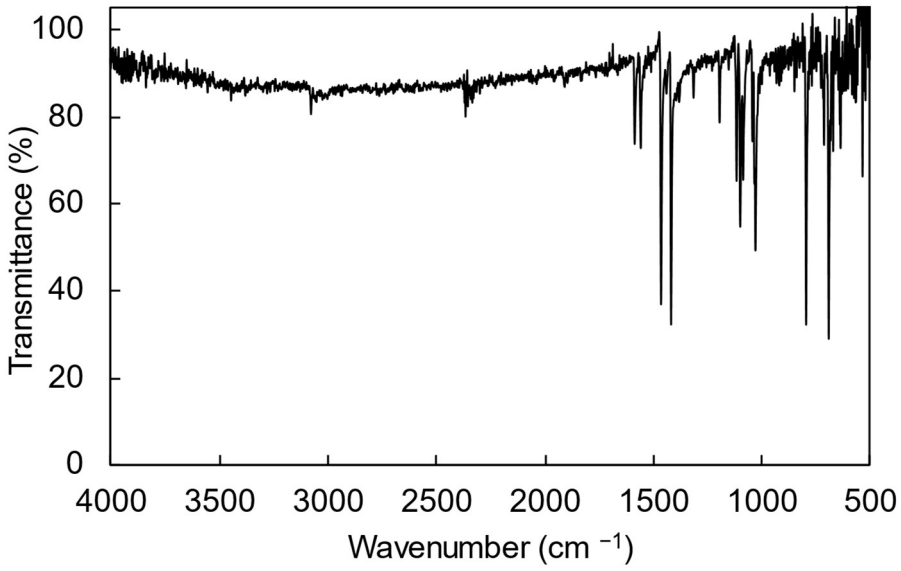

Figure S23 FT-IR spectra (KBr) of the CuI(3-BrPy) powder prepared by the reaction in suspension.

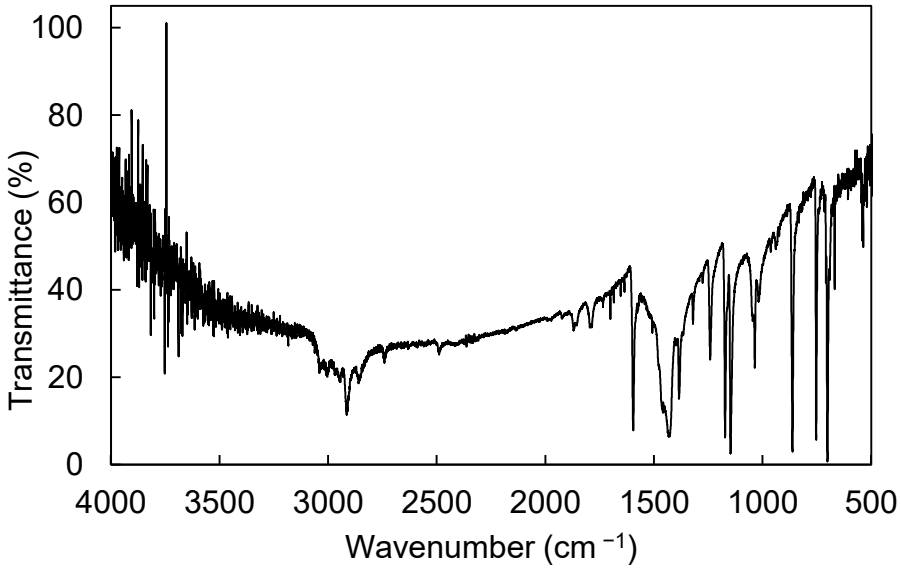

Figure S24 FT-IR spectra (KBr) of the CuI(3,5-Me_2Py) powder prepared by the reaction in suspension.

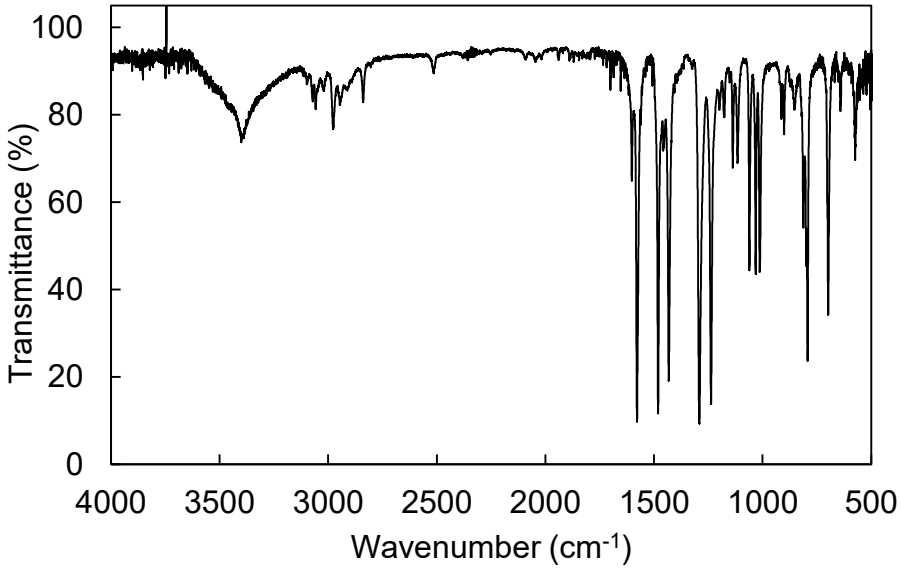

Figure S25 FT-IR spectra (KBr) of the CuCl(3-MeOPy) powder prepared by the reaction with with 2.7 equivalents of the pyridine ligand in suspension.

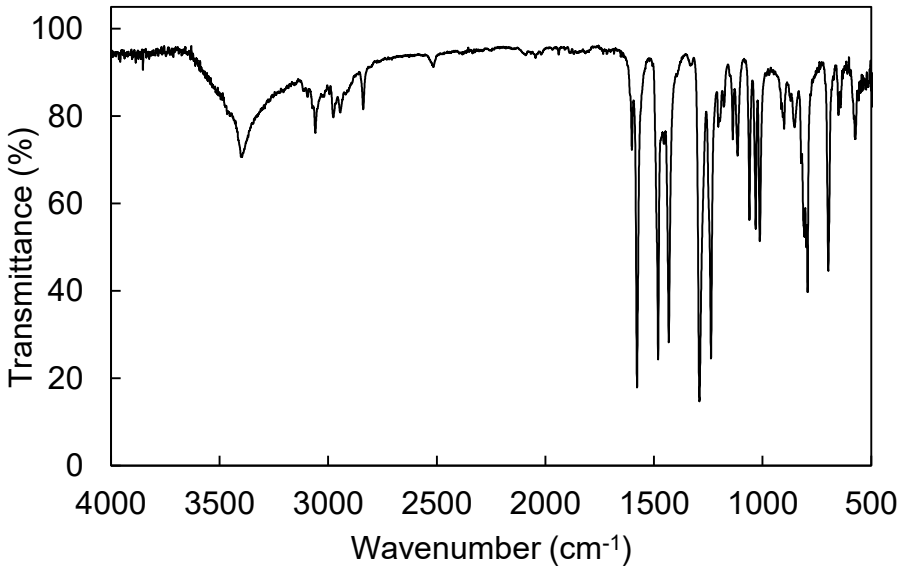

Figure S26 FT-IR spectra (KBr) of the CuCl(3-MeOPy) powder prepared by the reaction with with 3.9 equivalents of the pyridine ligand in suspension.

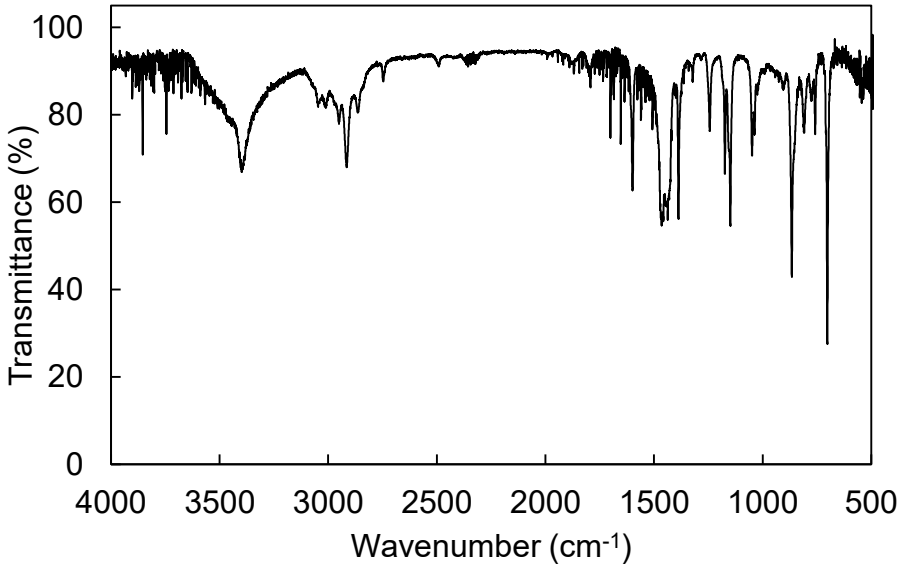

Figure S27 FT-IR spectra (KBr) of the CuCl(3,5-Me_2Py) powder prepared by the reaction with 1.0 equivalent of the pyridine ligand in suspension.

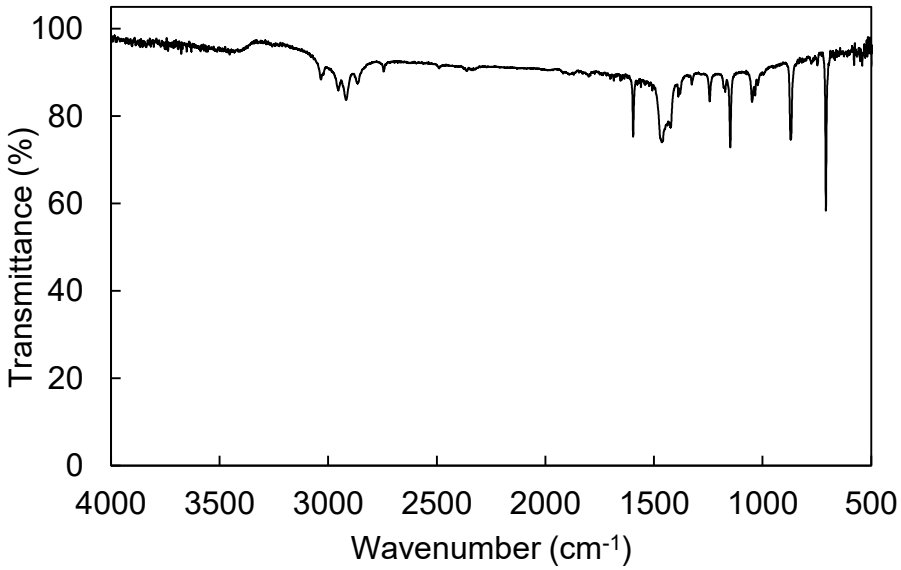

Figure S28 FT-IR spectra (KBr) of the CuCl(3,5-Me_2Py) powder prepared by the reaction with 3.6 equivalents of the pyridine ligand in suspension.

5. Thermogravimetric Data

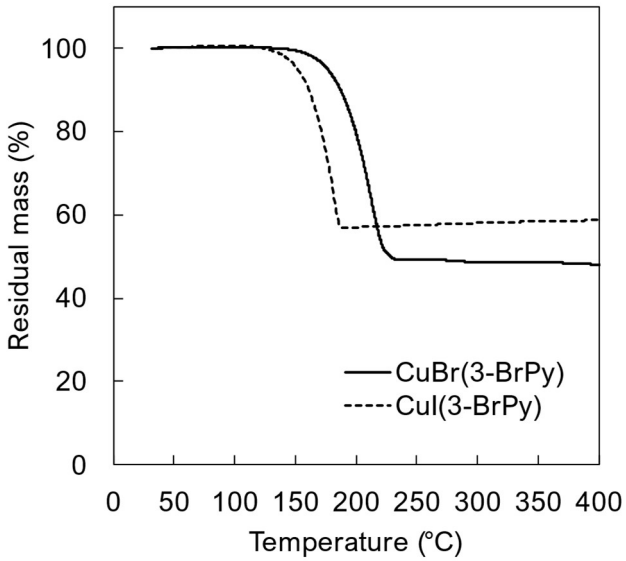

Figure S29 TG curves of the 3-bromopyridine complexes obtained by reaction in suspensions. The graph legend indicates the product.

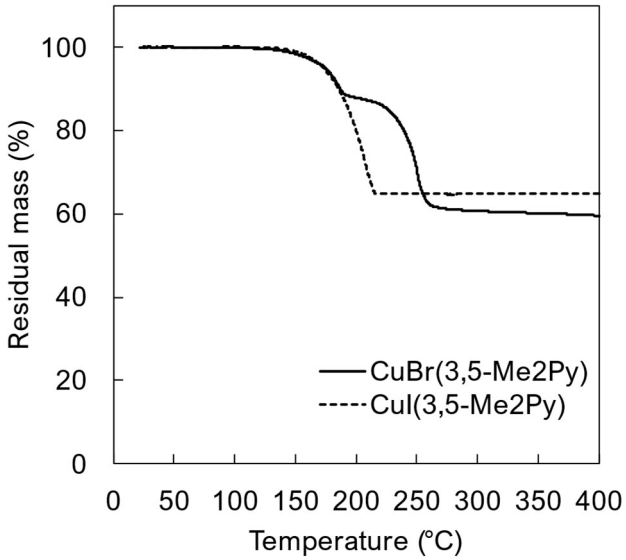

Figure S30 TG curves of the 3,5-dimethylpyridine complexes obtained by reaction in suspensions. The graph legend indicates the product.

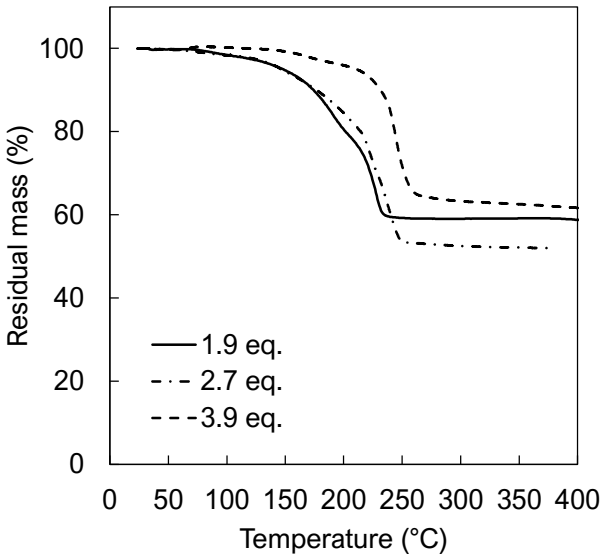

Figure S31 TG curve of the CuCl(3-MeOPy) powder obtained by the reaction with the different equivalent of the pyridine ligand in suspensions. The graph legend indicates the equivalents of 3-methoxypyridine used.

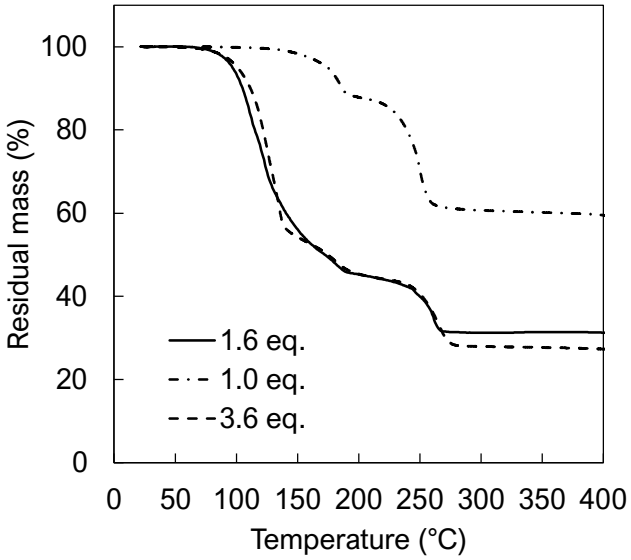

Figure S32 TG curves of the CuCl(3,5-Me_2Py) powder obtained by reaction with the different equivalent of the pyridine ligand in suspensions. The graph legend indicates the equivalents of 3,5-dimethylpyridine used.

6. Luminescence properties

6.1. Luminescent properties of CuI(3,5-Me_2Py) CP powder

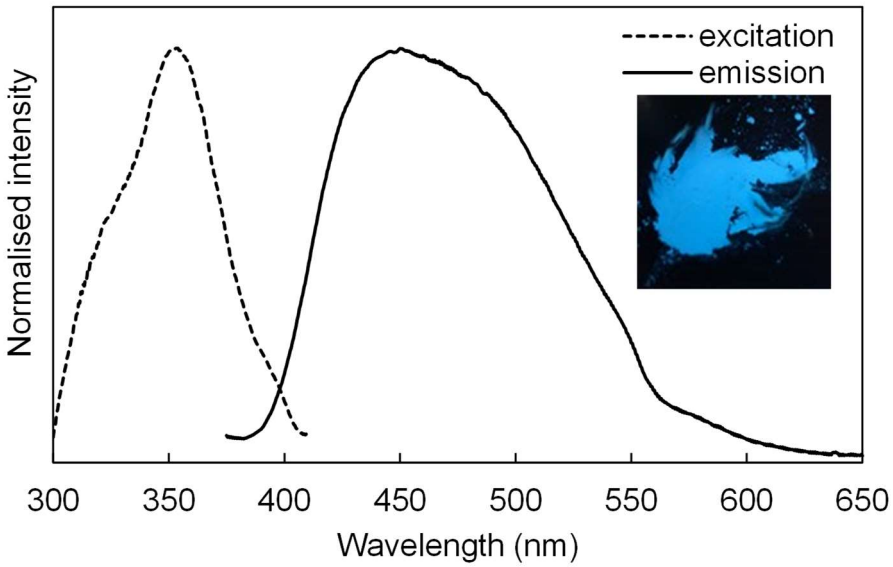

Figure S33 Excitation and emission spectra of the CuI(3,5-Me_2Py) powder prepared by the reaction in suspension. λ_{ex} = 350 nm, λ_{em} = 450 nm, Φ = 15%.

6.2. Luminescent properties of powders consist of some components

Luminescent properties of complexes consist of some components were shown in Table S10. Excitation and emission spectra were shown in Figure S34–Figure S40. Quantum yield was not evaluated because those products consist of some component.

Table S10 Luminescence properties of all resultant complexes consist of some component.

Products	λ_{ex} (nm)	λ_{em} (nm)
CuCl(3-H_2NCOPy)	370	480
CuCl(3-NH_2Py)	370	560
CuCl(4-CNPy)	390	580
CuCl(2-H_2CCHPy)	430	560
CuCl(3-MeOPy)	330	540
CuCl(3,5-Me_2Py)	390	540
CuBr(3,5-Me_2Py)	345	510

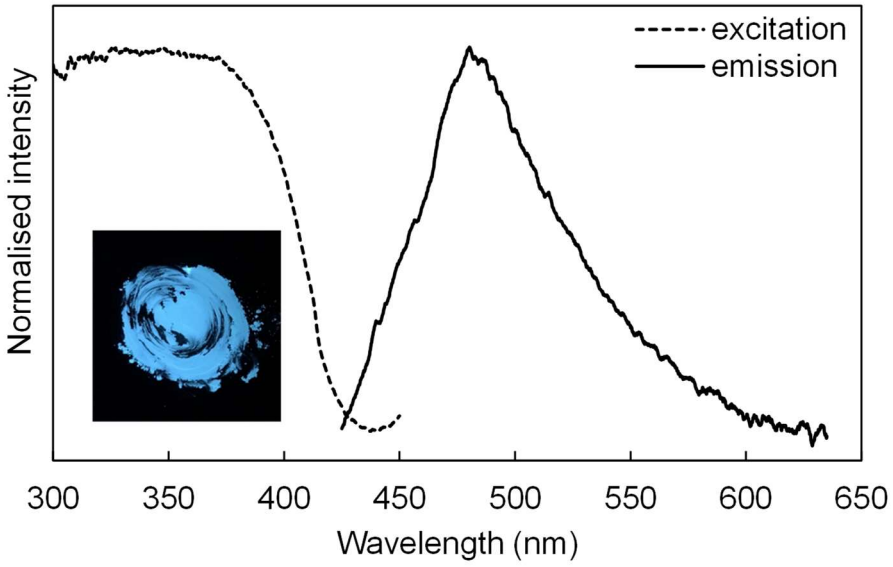

Figure S34 Excitation and emission spectra of the CuCl(3-H_2NCOPy) powder prepared by the reaction in suspension.

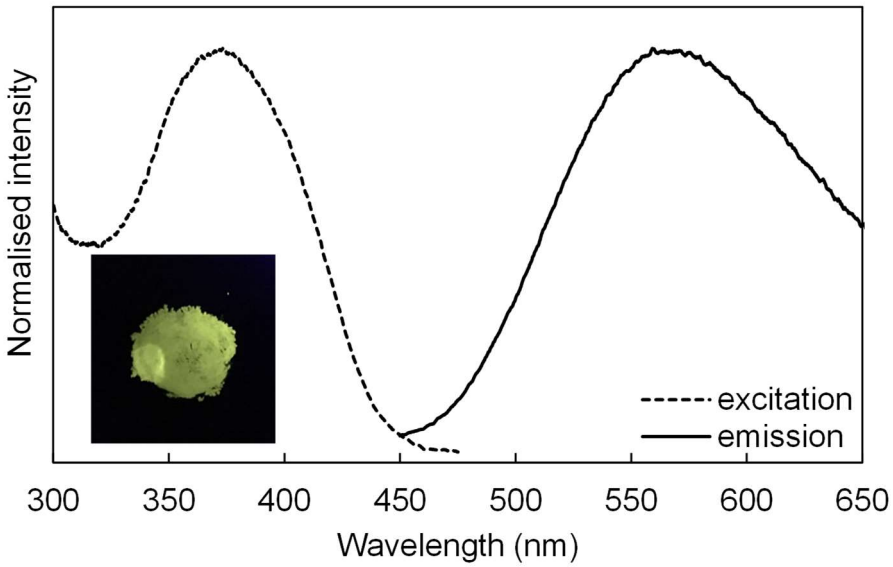

Figure S35 Excitation and emission spectra of the CuCl(3-NH_2Py) powder prepared by the reaction in suspension.

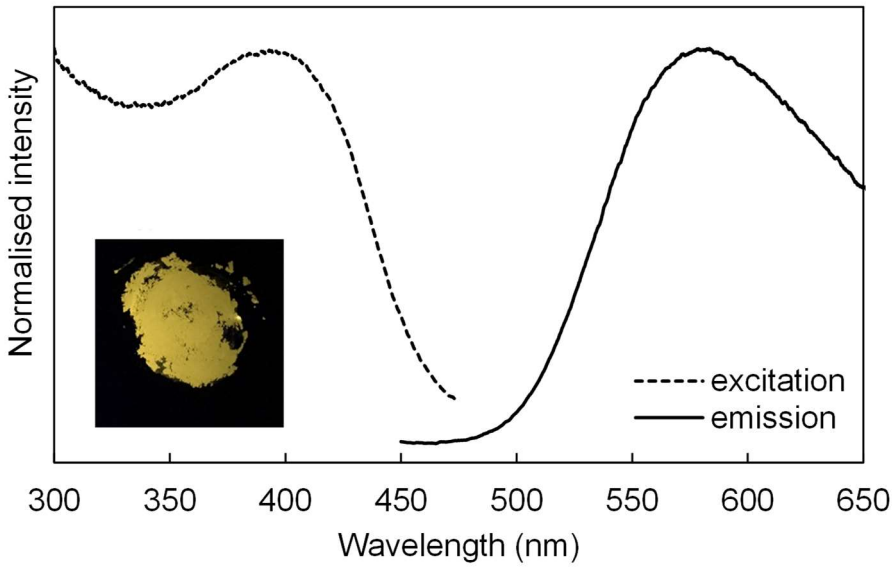

Figure S36 Excitation and emission spectra of the CuCl(4-CNPy) powder prepared by the reaction in suspension.

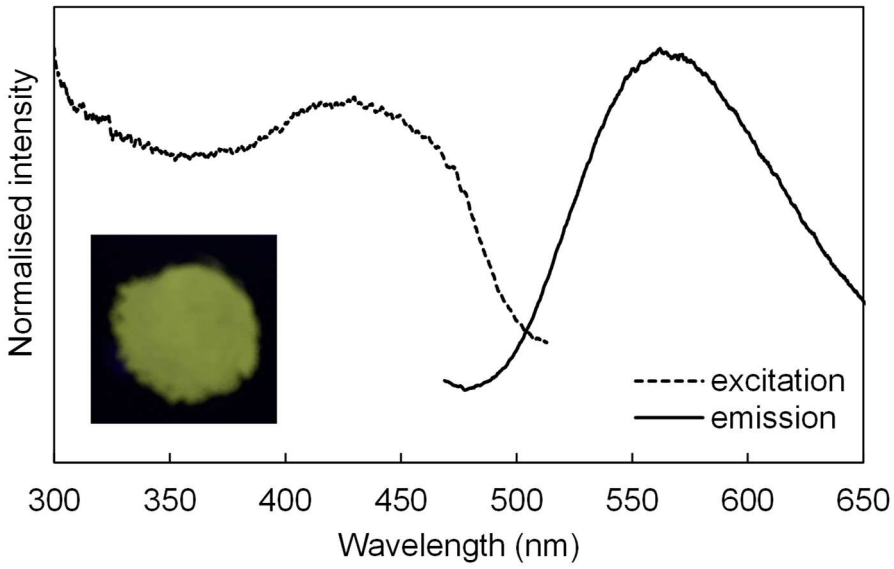

Figure S37 Excitation and emission spectra of the CuCl(2-H_2CCHPy) powder prepared by the reaction in suspension.

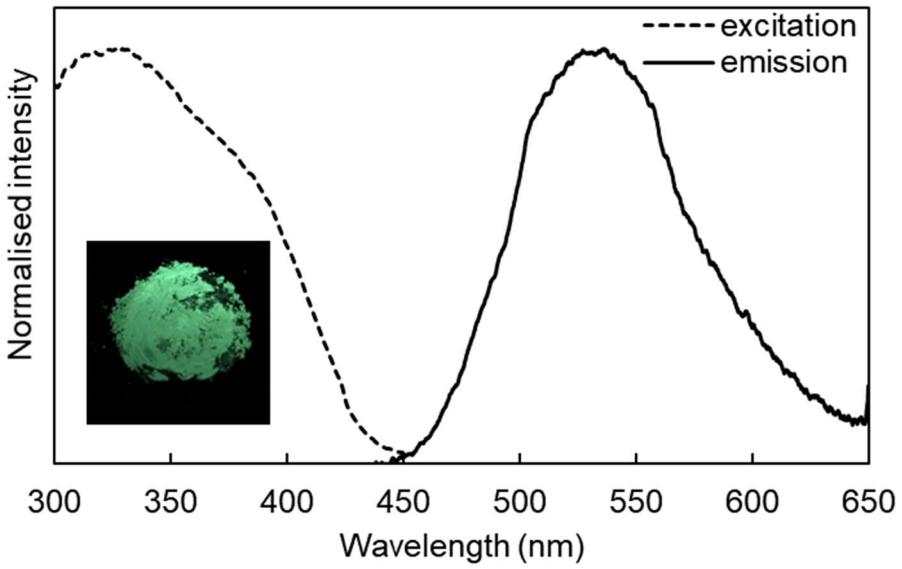

Figure S38 Excitation and emission spectra of the CuCl(3-MeOPy) powder prepared by the reaction in suspension.

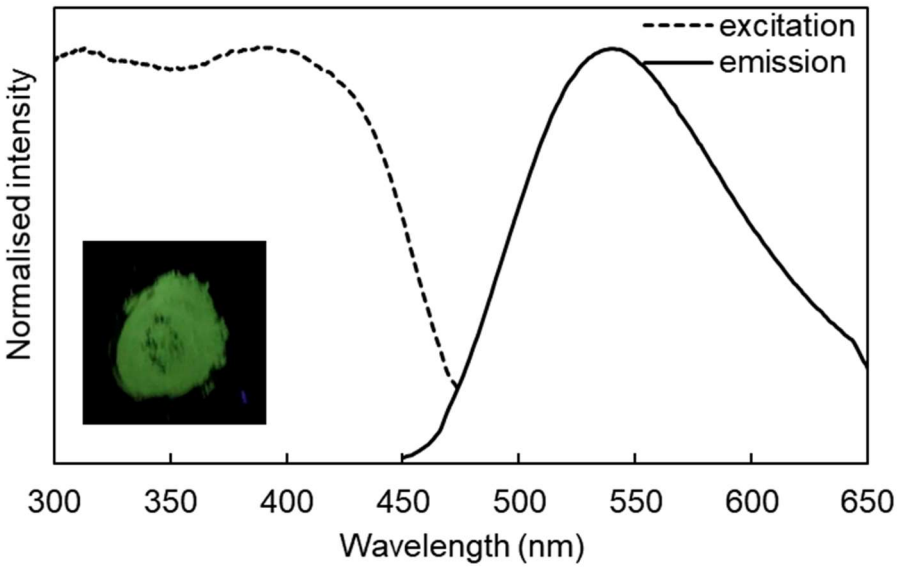

Figure S39 Excitation and emission spectra of the CuCl(3,5-Me_2Py) powder prepared by the reaction in suspension.

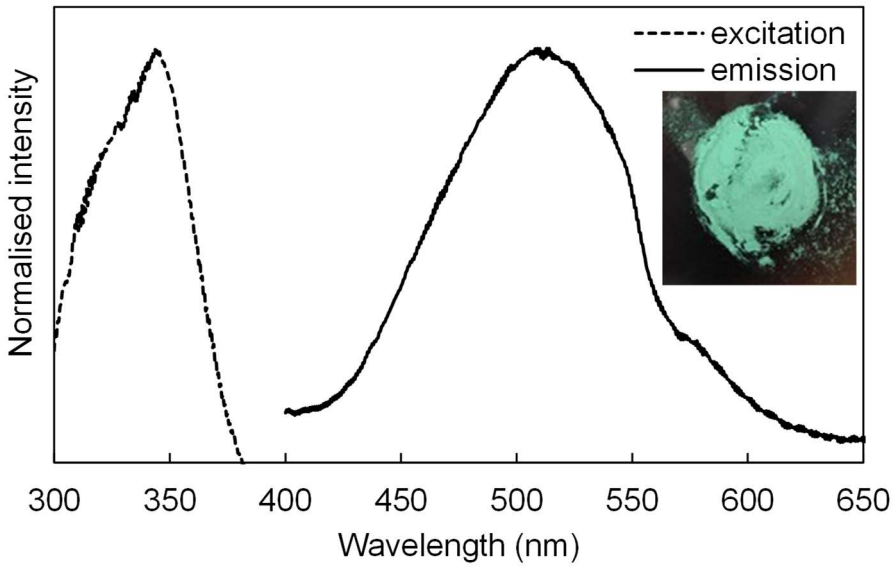

Figure S40 Excitation and emission spectra of the CuBr(3,5-Me_2Py) powder prepared by the reaction in suspension.

6.3. Luminescent properties of powders obtained with different equivalents of ligand in the synthesis

Table S11 Luminescence properties of complexes synthesised with changed equivalent of pyridine ligand.

Products	Equivalents of pyridine ligand	λ_{ex} (nm)	λ_{em} (nm)
CuCl(3-MeOPy)	2.7	350	520
CuCl(3,5-Me_2Py)	1.0	350	520
	3.6	350	525

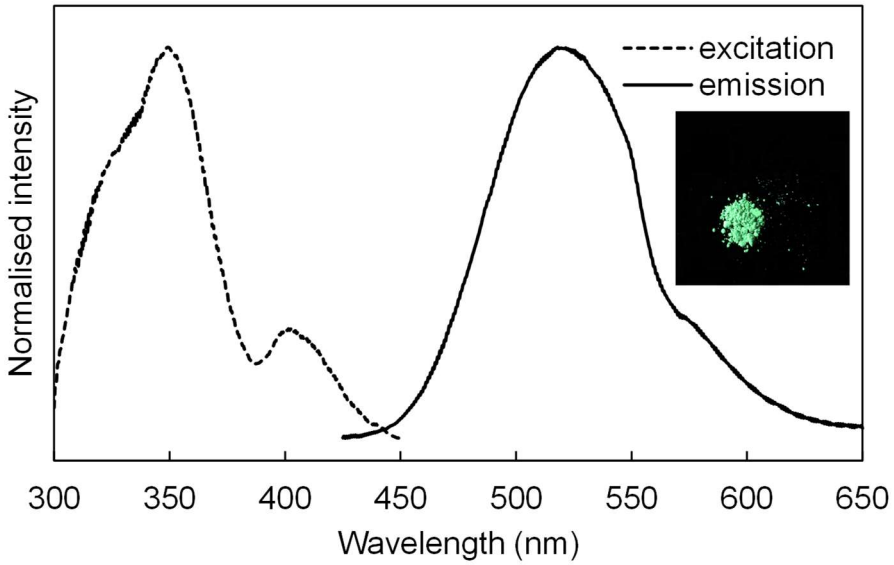

Figure S41 Excitation and emission spectra of the CuCl(3-MeOPy) powder prepared by the reaction with 2.7 equivalents of the pyridine ligand in suspension.

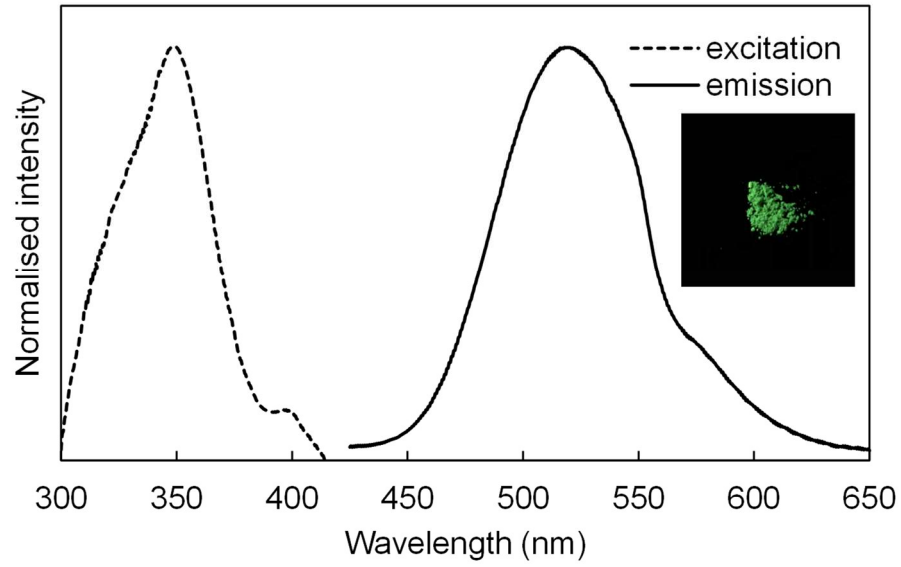

Figure S42 Excitation and emission spectra of the CuCl(3,5-Me_2Py) powder prepared by the reaction with 1.0 equivalents of the pyridine ligand in suspension.

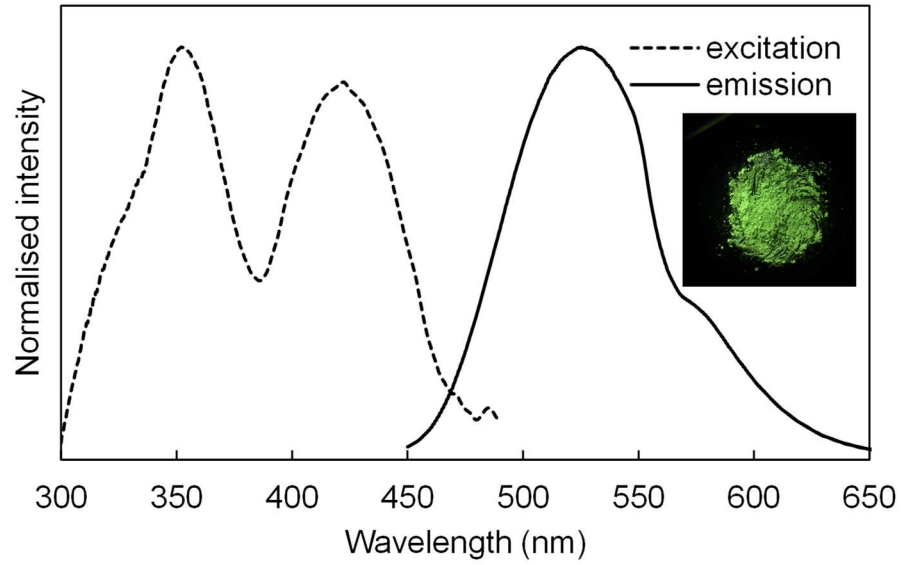

Figure S43 Excitation and emission spectra of the CuCl(3,5-Me_2Py) powder prepared by the reaction with 3.6 equivalents of the pyridine ligand in suspension. λ_{ex} = 350 nm, λ_{em} = 575 nm, Φ = 41%.

7. Simulation of Absorption Spectra

The XMLCT is a charge transfer excitation, and it is difficult to calculate the transition energy by TDDFT computation using the GGA functional [S13]. In general, too long wavelength is predicted. The transition energy of the charge transfer state is improved using the long-range corrected DFT (LC-DFT) in the case of the molecular system [S14]. However, the calculation using the LC-DFT for the periodic system still time-consuming and under development due to the exact exchange calculation difficulty. Although the description of charge transfer excitation wavelength is insufficient, in this study, TDDFT (TDDFPT) calculation was performed using the PBE functional, which is a GGA functional. UV-vis absorption spectra were simulated by the Davidson-like algorithm implemented in turboTDDFT code, a part of the Quantum ESPRESSO package. Based on the optimised structure, the UV-vis spectra were calculated using the SCF density obtained PBE functional and ultrasoft pseudopotentials (cutoff 40 Ry) using the reciprocal lattice sampled at the Γ point. For the simulation of UV-vis absorption spectra, 48 eigenstates were examined. The range of simulation is from 0.10 Ry to 0.31 Ry. The lowest excitation state was summarised in Table S12–Table S14. Those results indicated that the lowest excitation state of all compounds can be assigned to HOCO–LUCO transition mainly. The simulated UV-vis spectra were shown in Figure S44. As described above, the transition wavelength that is too long was predicted.

Table S12 Lowest excitation state of CuCl(3-BrPy).

Energy (Ry)	Wavelength (nm)	Principle components[a]			
		Occ.	Virt.	FX	FY
0.122	746	52	2	0.133	0.0170
		54	1	0.982	−0.0188

[a] Occupied orbital 54 corresponds to HOCO, and virtual orbital 1 corresponds to LUCO.

Table S13 Lowest excitation state of CuBr(3-BrPy).

Energy (Ry)	Wavelength (nm)	Principle components[a]			
		Occ.	Virt.	FX	FY
0.127	719	107	3	0.202	0.00125
		108	1	0.977	−0.00207

[a] Occupied orbital 108 corresponds to HOCO, and virtual orbital 1 corresponds to LUCO.

Table S14 Lowest excitation state of CuI(3-BrPy).

Energy (Ry)	Wavelength (nm)	Principle components[a]			
		Occ.	Virt.	FX	FY
0.118	775	107	1	-0.129	0.00043
		107	3	0.380	0.00196
		108	1	0.813	−0.00297
		108	2	0.409	−0.00151

[a] Occupied orbital 108 corresponds to HOCO, and virtual orbital 1 corresponds to LUCO.

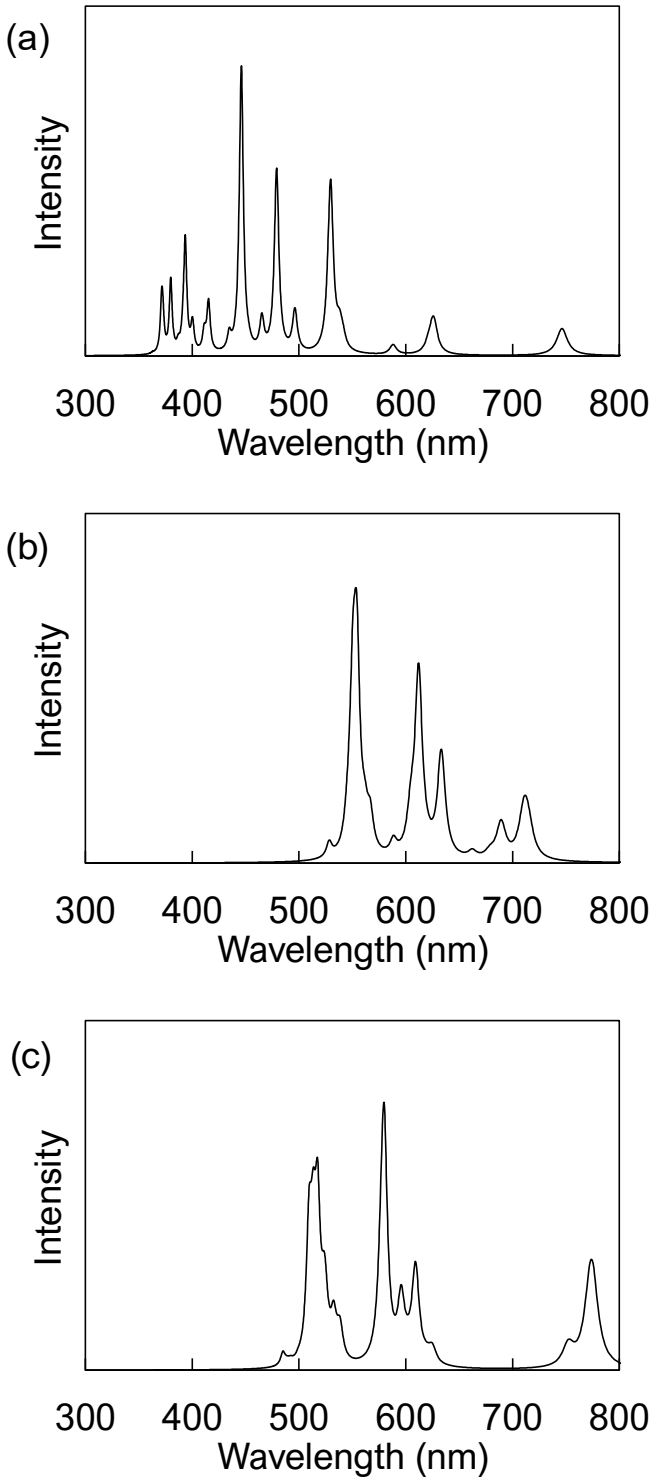

Figure S44 Simulated UV-vis absorption spectra of (a) CuCl(3-BrPy) CP; (b) CuBr(3-BrPy); (c) CuI(3-BrPy). A factor of 0.001 Ry broadened those spectra.

8. Relationship between Luminescence Maxima and Frontier Orbitals

The frontier orbital level of pyridine ligands was calculated at B3LYP-D3(BJ)/def2-SVP level of theory using ORCA 4.2.1 [S15].

Table S15 Frontier orbital level of pyridine ligands.

Compound	HOMO (eV)	LUMO (eV)
2-bromopyridine	−6.96	−1.12
2-vinylpyridine	−6.50	−1.31
3-aminopyridine	−5.76	−0.45
3-bromopyridine	−7.00	−1.13
3-methoxypyridine	−6.34	−0.64
3-vinylpyridine	−6.51	−1.33
4-cyanopyridine	−7.57	−2.17
3,5-dichloropyridine	−7.15	−1.39
3,5-dimethylpyridine	−6.67	−0.48
Isoquinoline	−6.35	−1.55
nicotinamide	−6.93	−1.41
pyridine	−6.88	−0.76

CuCl(3-BrPy) and CuCl(3-MeOPy) complex, which has the same structure, show a red shift of the emission wavelength due to the increase of LUMO and HOMO. However, totally no clear relationship was obtained. This result suggests that the structure of those complexes is different.

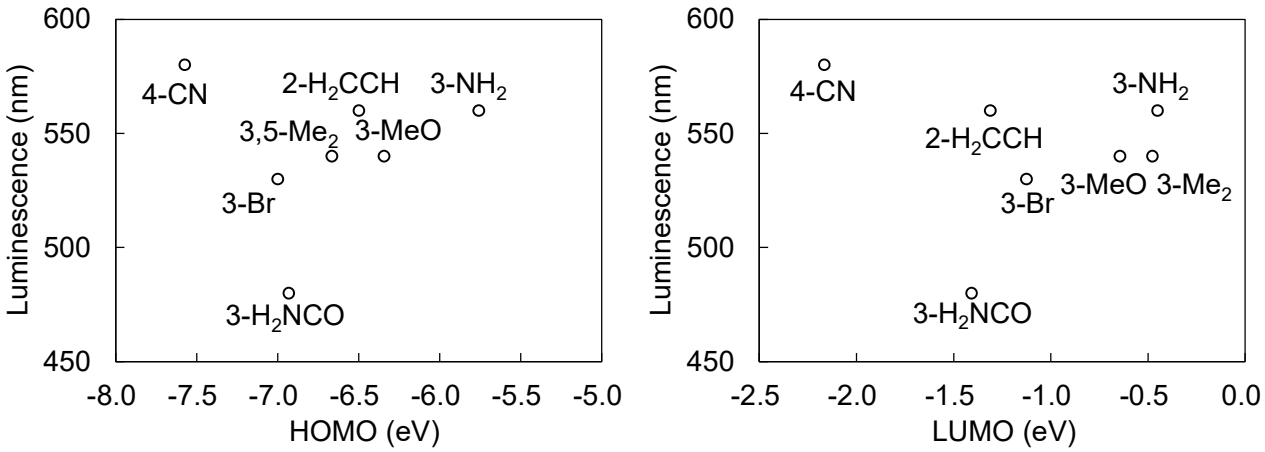

Figure S45 Relationship between luminescence maxima and frontier orbitals (HOMO or LUMO).

9. References

[S1] L. M. Engelhardt, P. C. Healy, J. D. Kildea and A. H. White, *Aust. J. Chem.*, 1989, **42**, 185–199.

[S2] J. M. Dyason, L. M. Engelhardt, P. C. Healy and A. H. White, *Aust. J. Chem.*, 1986, **39**, 1043–1051.

[S3] H. D. Hardt and H. Gechnizdjani, *Z. Anorg. Allg. Chem.*, 1973, **397**, 23–30.

[S4] A. J. Graham, P. C. Healy, J. D. Kildea and A. H. White, *Aust. J. Chem.*, 1989, **42**, 177–184.

[S5] G. W. Watt and W. R. Strait, *J. Inorg. Nucl. Chem.*, 1972, **34**, 1657–1662.

[S6] J. C. Rubim and O. Sala, *J. Mol. Struct.*, 1986, **145**, 157–172.

[S7] A. U. Malik, *Z. Anorg. Allg. Chem.*, 1966, **344**, 107–112.

[S8] J. A. Campbell, C. L. Raston and A. H. White, *Aust. J. Chem.*, 1977, **30**, 1937–1945.

[S9] J. Li, X. Zhang, G. Z. Wei and W. Liu, PCT application, WO/2014/201377.

[S10] W. Liu, D. Banerjee, F. Lin and J. Li, *J. Mater. Chem. C*, 2019, **7**, 1484–1490.

[S11] X. Zhang, W. Liu, G. Z. Wei, D. Banerjee, Z. Hu and J. Li, *J. Am. Chem. Soc.*, 2014, **136**, 14230–14236.

[S12] N. Kitada and T. Ishida, *CrystEngComm*, 2014, **16**, 8035–8040.

[S13] T. Ziegler, M. Seth, M. Krykunov, J. Autschbach and F. Wang, *J. Mol. Struct. THEOCHEM*, 2009, **914**, 106–109.

[S14] Y. Tawada, T. Tsuneda, S. Yanagisawa, T. Yanai and K. Hirao, *J. Chem. Phys*, 2004, **120**, 8425–8433.

[S15] F. Neese, *WIREs Comput. Mol. Sci.*, 2018, **8**, e1327.